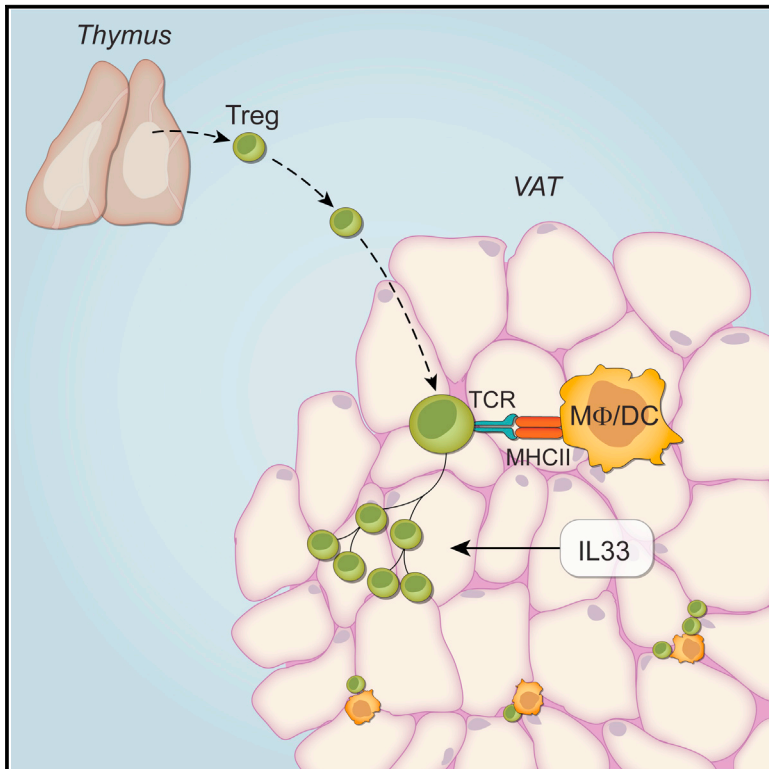


# Cell Metabolism

## Antigen- and Cytokine-Driven Accumulation of Regulatory T Cells in Visceral Adipose Tissue of Lean Mice

### Graphical Abstract



### Authors

Dmitriy Kolodin,  
Nicolas van Panhuys, ...,  
Christophe Benoist, Diane Mathis

### Correspondence

cbdm@hms.harvard.edu

### In Brief

Kolodin et al. carefully characterize the origins of visceral adipose tissue regulatory T cells, which have beneficial metabolic effects in lean mice. They show that these cells are seeded from the thymus soon after birth and that their accumulation depends on local antigens and mediators, notably interleukin-33.

### Highlights

- VAT Tregs are generated in the thymus in the first weeks of life
- VAT Tregs of lean mice show clonal micro-expansions and enhanced survival rates
- Retention/accumulation depends on in situ recognition of an MHCII-restricted antigen(s)
- The VAT Treg population of lean mice depends on and is potently expanded by IL-33



# Antigen- and Cytokine-Driven Accumulation of Regulatory T Cells in Visceral Adipose Tissue of Lean Mice

Dmitriy Kolodin,<sup>1</sup> Nicolas van Panhuys,<sup>2</sup> Chaoran Li,<sup>1</sup> Angela M. Magnuson,<sup>1</sup> Daniela Cipolletta,<sup>1</sup> Christine M. Miller,<sup>3</sup> Amy Wagers,<sup>3,4,5</sup> Ronald N. Germain,<sup>2</sup> Christophe Benoist,<sup>1,6</sup> and Diane Mathis<sup>1,6,\*</sup>

<sup>1</sup>Department of Microbiology and Immunobiology, Harvard Medical School, Boston, MA 02115, USA

<sup>2</sup>Lymphocyte Biology Section, Laboratory of Systems Biology, National Institute of Allergy and Infectious Diseases, NIH, Bethesda, MD 20892, USA

<sup>3</sup>Joslin Diabetes Center, Boston, MA 02215, USA

<sup>4</sup>Department of Stem Cell and Regenerative Biology, Harvard University, Cambridge, MA 02138, USA

<sup>5</sup>Howard Hughes Medical Institute, Chevy Chase, MD 20815, USA

<sup>6</sup>Evergrande Center for Immunologic Diseases, Harvard Medical School and Brigham and Women's Hospital, Boston MA 02115, USA

\*Correspondence: [cbdm@hms.harvard.edu](mailto:cbdm@hms.harvard.edu)

<http://dx.doi.org/10.1016/j.cmet.2015.03.005>

## SUMMARY

A unique population of Foxp3<sup>+</sup>CD4<sup>+</sup> regulatory T (Treg) cells, with a distinct transcriptome and antigen-receptor repertoire, resides in visceral adipose tissue (VAT) of lean individuals. These cells regulate local inflammation and both local and systemic metabolic indices. Here we focus on expansion of the VAT Treg compartment in aging lean mice—assessing these cells' phenotypic conversion from conventional CD4<sup>+</sup> T cells, influx from lymphoid organs, and local population dynamics. Our findings establish that the VAT Treg compartment is seeded from thymocytes generated during the first weeks of life and expands beyond 10 weeks of age due to indolent proliferation, of certain clones in particular, coupled with enhanced survival. Accumulation of VAT Tregs depends on the antigen(s) presented by MHC class-II molecules and soluble mediators, notably interleukin(IL)-33. Addressing such factors therapeutically promises novel approaches for harnessing Tregs to stem the growing epidemic of obesity and consequent metabolic abnormalities.

## INTRODUCTION

Visceral adipose tissue (VAT), notably the epididymal fat depot in mice and omental depot in humans, is a site where metabolic and immunologic processes interplay (Osborn and Olefsky, 2012; Mathis, 2013). The epididymal fat of lean mice is maintained in an anti-inflammatory state, kept in check by cells of both the innate and adaptive immune systems, notably anti-inflammatory macrophages (MFs) and regulatory T (Treg) cells. With nutrient overload, and the consequent onset of obesity, this fat depot takes on a pro-inflammatory tenor, hosting a variety of innate and adaptive effector-cell types, such as neutrophils, pro-inflammatory MFs, CD8<sup>+</sup> T lymphocytes, and T helper

(Th)1 cells. Given its inaccessibility, few studies have been done on human omental fat, but some of the same immunocyte types infiltrate this depot, notably MFs and Tregs, and this depot has been the one most frequently associated with metabolic abnormalities. The anti-/pro-inflammatory balance in VAT is a critical determinant of metabolic health, its dysregulation promoting insulin resistance, type-2 diabetes, cardiovascular disorders, and fatty liver.

Foxp3<sup>+</sup>CD4<sup>+</sup> Treg cells are critical regulators of the inflammatory state of murine VAT (Feuerer et al., 2009), perhaps not surprising given that this lymphocyte subset controls most types of immune responses (Josefowicz et al., 2012a). In lean mice, visceral adipose depots harbor a population of Treg cells very different from standard lymphoid tissue Tregs according to a number of criteria. The fractional representation of VAT Tregs (40%–80% of CD4<sup>+</sup> T cells) is unusually high, rising well above that of the circulating Treg pool (5%–15%). In addition, the transcriptome of VAT Tregs from lean mice is distinct from that of their lymphoid tissue counterparts, showing enrichment in transcripts encoding certain chemokine receptors, (e.g., CCR1 and CCR2), a few cytokines (e.g., unusually high levels of IL-10), and a set of proteins involved in lipid metabolism (e.g., CD36, Dgat1, and Ldlr). Lastly, adipose tissue and lymphoid tissue Tregs display distinct repertoires of antigen-specific receptors (T cell receptors [TCRs]). Obesity is accompanied by a striking drop in the population of Treg cells in VAT, but not elsewhere, and systemic reduction or augmentation of Tregs increases or decreases adipose tissue inflammation and insulin resistance, respectively (Feuerer et al., 2009; Eller et al., 2011), arguing for a significant role for Treg cells in regulating metabolic processes.

A major determinant of the VAT Treg gene expression signature in lean mice is a transcription factor important in the differentiation and function of adipocytes, PPAR- $\gamma$  (Cipolletta et al., 2012). Treg-specific ablation of *Pparg* resulted in depletion of VAT, but not lymphoid tissue, Treg cells in mice fed a normal diet (ND). Conversely, injection of the PPAR $\gamma$  agonist pioglitazone into mice maintained on a high-fat diet (HFD), and thereby impoverished in VAT Treg cells, greatly expanded the VAT, but not lymphoid tissue, Treg population. Interestingly, many of the

well-known insulin-sensitizing effects of pioglitazone were blunted in mice lacking PPAR $\gamma$  specifically in Treg cells.

These findings establish the importance of the VAT Treg compartment in regulating local and systemic metabolic processes but leave open the question of how this unique population accumulates in lean individuals. We previously reported that expansion of the VAT Treg pool in lean mice becomes noticeable at 10–15 weeks of age in our mouse colony and peaks at 20–25 weeks (Feuerer et al., 2009). Here we explore three potential explanations for this accumulation: Treg phenotypic conversion from conventional CD4<sup>+</sup> T (Tconv) cells, influx of Treg immigrants from the lymphoid organs, and local dynamics of the VAT Treg population.

## RESULTS

### No Evidence of VAT Treg Conversion from Tconv Cells

Most Foxp3<sup>+</sup>CD4<sup>+</sup> Treg cells are exported as such from the thymus (and are termed tTregs). However, they can also be generated in the periphery (pTregs) or in vitro (iTregs) by conversion from Foxp3<sup>-</sup>CD4<sup>+</sup> Tconv cells; for example, in the presence of transforming growth factor (TGF)- $\beta$ . pTreg cells, notably those residing in the intestinal lamina propria (Josefowicz et al., 2012b) and placenta (Samstein et al., 2012), can make an important contribution to the regulation of immune responses. Our previously reported sequencing data, discerning no overlap between the TCR repertoires of VAT Treg cells and VAT or lymphoid tissue Tconv cells in a mouse line engineered to express a drastically reduced set of *Tcra* and *Tcrb* gene segments, argued against a substantial population of converted VAT Tregs (Feuerer et al., 2009). However, given the (overly) simplified model employed in those studies, it was important to extend this conclusion to a normal setting.

First, we examined the expression of markers purported to distinguish between tTregs and pTregs, namely Helios and Neuropilin (Nrp)-1 (Thornton et al., 2010; Weiss et al., 2012). These are not perfect markers, but in general, pTregs have a Helios<sup>lo</sup>Nrp-1<sup>lo</sup> phenotype while tTregs express high levels of both proteins. Most Treg cells in VAT, as in lymphoid tissues, had a Helios<sup>hi</sup>Nrp-1<sup>hi</sup> phenotype; in fact, the fraction of Helios<sup>+</sup> Tregs in VAT was even higher than that in the spleen and lymph nodes (LNs), approaching 100% (Figures 1A and 1B). These findings held at both early and late stages of VAT Treg cell accumulation in C57BL/6 (B6) mice (i.e., at both 15 and > 25 weeks of age).

Second, we searched for signs of Tconv  $\rightarrow$  Treg phenotypic conversion in the transcriptome of VAT Treg cells. Converted Treg gene expression signatures were derived from multiple well-studied in vivo and in vitro models: Tconv  $\rightarrow$  Treg conversion by (1) low-dose administration of antigen (influenza hemagglutinin [HA] peptide) through delivery to dendritic cells (DCs) as a fusion with the monoclonal antibody (mAb) DEC205; (2) transfer of naive Tconv cells into lymphopenic Rag-deficient mice, thereby inducing homeostatic proliferation; and (3) activation of cultured Tconv cells in the presence of IL-2 and TGF- $\beta$ . Microarray data on pTregs and iTregs generated in these models and on VAT and control LN Treg cells have been reported previously (Feuerer et al., 2010; Cipolletta et al., 2012); details on refinement of the pTreg and iTreg “up” and “down” signatures can be found in the Supplemental Experimental Procedures, as exemplified in

Figure S1. Superimposition of these signatures onto volcano plots comparing the transcriptomes of VAT and LN Treg cells from >25-week-old B6 mice revealed no significant over- or under-representation in VAT Tregs (Figure 1C), arguing against a substantial pTreg contribution to this compartment. Similar results were obtained with VAT and LN Treg data from 5- and 14-week-old mice (not shown).

Third, we performed a transfer experiment to test directly whether Tconv cells could turn on Foxp3 expression to become VAT Tregs. Five million Tconv cells (GFP<sup>-</sup>CD4<sup>+</sup>CD45.1<sup>+</sup>) were sorted from spleens of 8-week-old Foxp3<sup>iGFP</sup> reporter mice and were transferred intravenously (iv) into lean 20-week-old CD45.2<sup>+</sup> congenic recipients. (By-far-insufficient numbers precluded the use of VAT Tconv donor cells). Four weeks later, we consistently saw a small population of donor-derived Treg cells (GFP<sup>+</sup>CD4<sup>+</sup>CD45.1<sup>+</sup>) in the spleen and LNs but did not detect them in VAT of any of the nine mice examined in multiple independent experiments; we did, however, find donor-derived Tconv cells (GFP<sup>-</sup>CD4<sup>+</sup>CD45.1<sup>+</sup>) (Figure 1D).

Thus, none of our current or past data provide evidence of VAT Treg conversion from Foxp3<sup>-</sup>CD4<sup>+</sup> Tconv cells. It might be worth mentioning that we could not use the pTreg-deficient CNS1 mutant mouse line of Rudensky and colleagues to address this issue because the Treg cells in those animals express a Foxp3-GFP fusion protein that inhibits their accumulation in VAT (Zheng et al., 2010; Darce et al., 2012) (data not shown).

### Little Contribution of Circulating Tregs to the VAT Compartment of Lean Mice

Another potential explanation for VAT Treg accumulation in older mice is that around 10 weeks of age VAT becomes more attractive to circulating Treg cells, which install there and undergo phenotypic adaptations. Therefore, we performed a series of experiments to assess the ability of Treg cells to migrate from the blood and peripheral lymphoid organs to VAT. A classical approach to address such an issue is by means of transfer experiments. A million GFP<sup>+</sup> splenic Treg cells were isolated from 8- to 10-week-old CD45.1<sup>+</sup>Foxp3<sup>iGFP</sup> donors and were iv injected into 20-week-old CD45.2<sup>+</sup> recipients. 4 weeks later, the contribution of donor Tregs to the spleen, LN, and VAT Treg compartments was assessed. While CD45.1<sup>+</sup> cells were readily detectable in the lymphoid organs, making up about 0.5% of the Treg population, significantly fewer were found in VAT (Figure 2A)—and most importantly, clearly not more.

Another, less invasive, approach made use of Kaede/B6 transgenic mice, which express a photoconvertible (green  $\rightarrow$  red) reporter in all cells under the dictates of  $\beta$ -actin gene promoter/enhancer elements (Tomura et al., 2008). Immunocytes present at a designated location can be innocuously photoconverted by applying violet light transcutaneously, and their migration can then be monitored for up to 2 weeks by ex vivo cytofluorimetry or fluorescence microscopy. We exposed cervical LNs (CLNs) to violet light, monitored the egress of CD4<sup>+</sup> T cell subsets from that site, and followed their immigration over the next 72 hr into VAT versus pooled axillary and inguinal LNs (A/ILNS), the latter sites reflective of steady-state circulation, and so used to calculate a “migration-ratio” that permits ready comparison of migration to a designated site vis-à-vis the general circulation (Figure 2B). Consistent with our previous findings (Morton

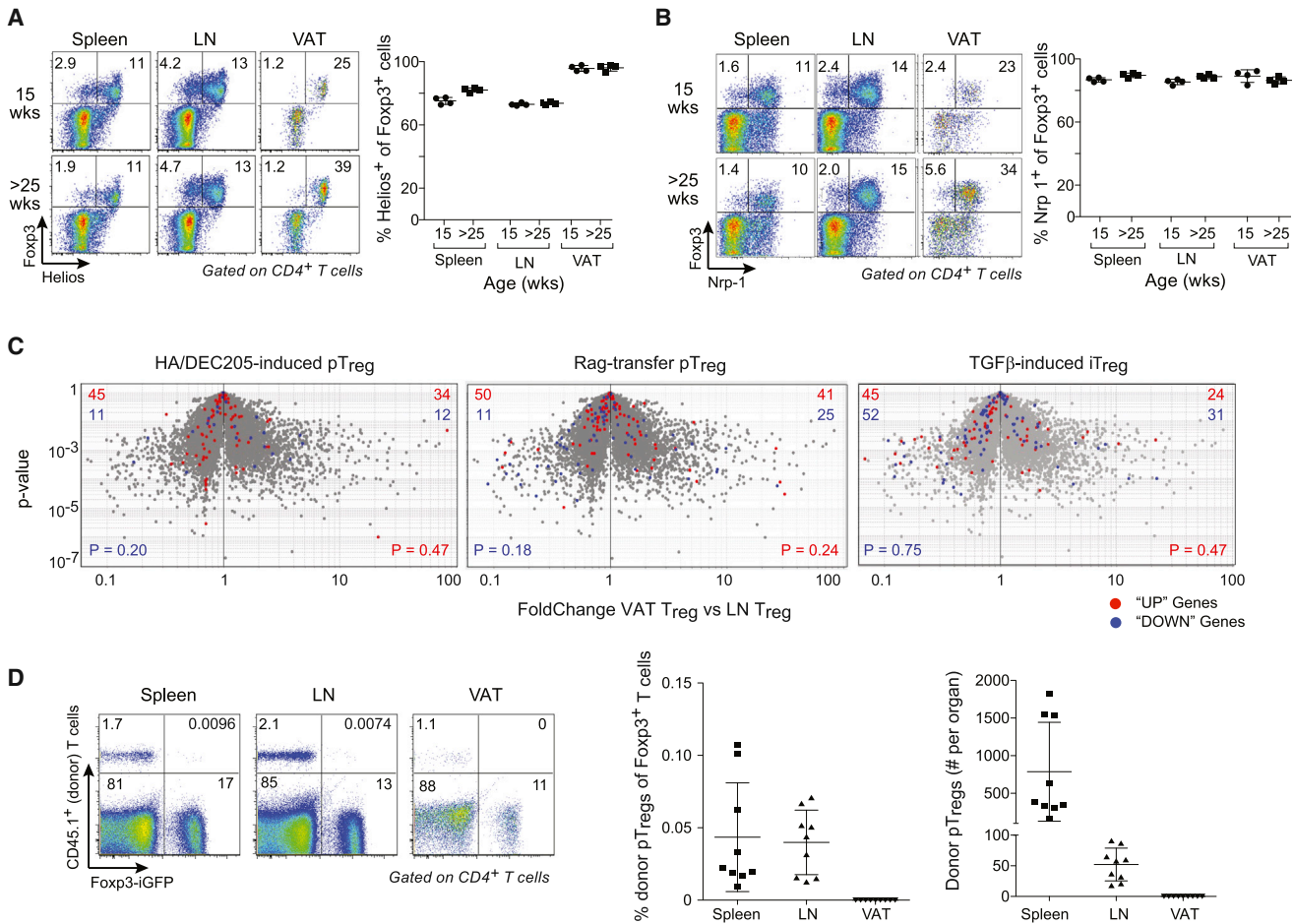


**Figure 1. No Evidence of VAT Treg Conversion from Tconv Cells**

(A and B) Marker expression. Left panels: representative cytofluorometric dot plots of Helios (A) or Nrp-1 (B) expression in CD4<sup>+</sup> T cell compartments of mice 15 or >25 weeks of age. Right panels: corresponding summary data pooled from two independent experiments.

(C) Transcriptome analysis. FC versus p value plots comparing transcriptomes of VAT and LN T<sub>regs</sub> isolated from 30-week-old mice (in triplicate). The indicated signatures, derived as detailed in the [Supplemental Experimental Procedures](#), were overlain on each plot. p values generated using the chi-square test.

(D) Transfer studies. Foxp3<sup>-</sup> Tconv cells from pooled spleen and LNs of CD45.1<sup>+</sup> Foxp3<sup>IGFP</sup> donors were iv transferred into CD45.2<sup>+</sup> Foxp3<sup>IGFP</sup> recipients, and analyzed 4 weeks later. Left panels: representative flow cytometry plots. Summary data for donor Treg percentage (center panels) and number (right) are also presented. Pooled data from three independent experiments. Mean ± SD.

[et al., 2014](#)), Tconv cells exited the CLNs more rapidly than did Treg cells (Figure 2C, left panel). In most mice, both Tconv and Treg cells migrated substantially less effectively to VAT than to lymphoid tissue (set at 1) (Figure 2C, right panel). This finding was true whether we looked early (16 weeks of age) or late (24 weeks) in the VAT Treg expansion phase (data not shown).

For a longer-term view, we turned to parabiosis experiments. 8-week-old B6.CD45.1 and B6.CD45.2 mice were conjoined, and the chimerism of various T cell compartments was examined 4 or 6 weeks later (Figure 2D). Admixture of the spleen Treg population approached 50:50 after 4 weeks of parabiosis (40%), and this mix was not significantly different 2 weeks later (43%). Chimerism of the VAT Treg compartment was low at both time points (17% and 24%), the values clearly diverging from their spleen counterparts. Later parabiosis experiments revealed that the majority of partner-derived Foxp3<sup>+</sup>CD4<sup>+</sup> cells found in VAT were circulating lymphoid-tissue-type Tregs, as they did

not express typical VAT Treg markers (e.g., Gata3 and Klr1) ([Cipolletta et al., 2012](#)) (data not shown).

### Micro-Expansions of VAT Treg Clones

Next, we explored the dynamics of the Treg population residing in VAT. Its accumulation could, in theory, reflect increased proliferation or slower turnover vis-à-vis lymphoid tissue Treg populations, or both. Proliferation was studied by quantifying incorporation of the nucleoside analog 5-ethynyl-20-deoxyuridine (EdU) and by staining for Ki67, a marker for cycling cells. A 4 hr in vivo pulse of EdU revealed a small population of dividing VAT Treg cells, similar to what was found for splenic Tregs—while there were significantly more (though still few) dividing cells in VAT at 15 to 16 weeks of age, this difference did not hold in older mice (Figure 3A). Significantly more Treg than Tconv cells were dividing in both spleen and VAT in both age groups. Ki67 staining, which labels cells at all but the G<sub>0</sub> phase of the cell cycle,

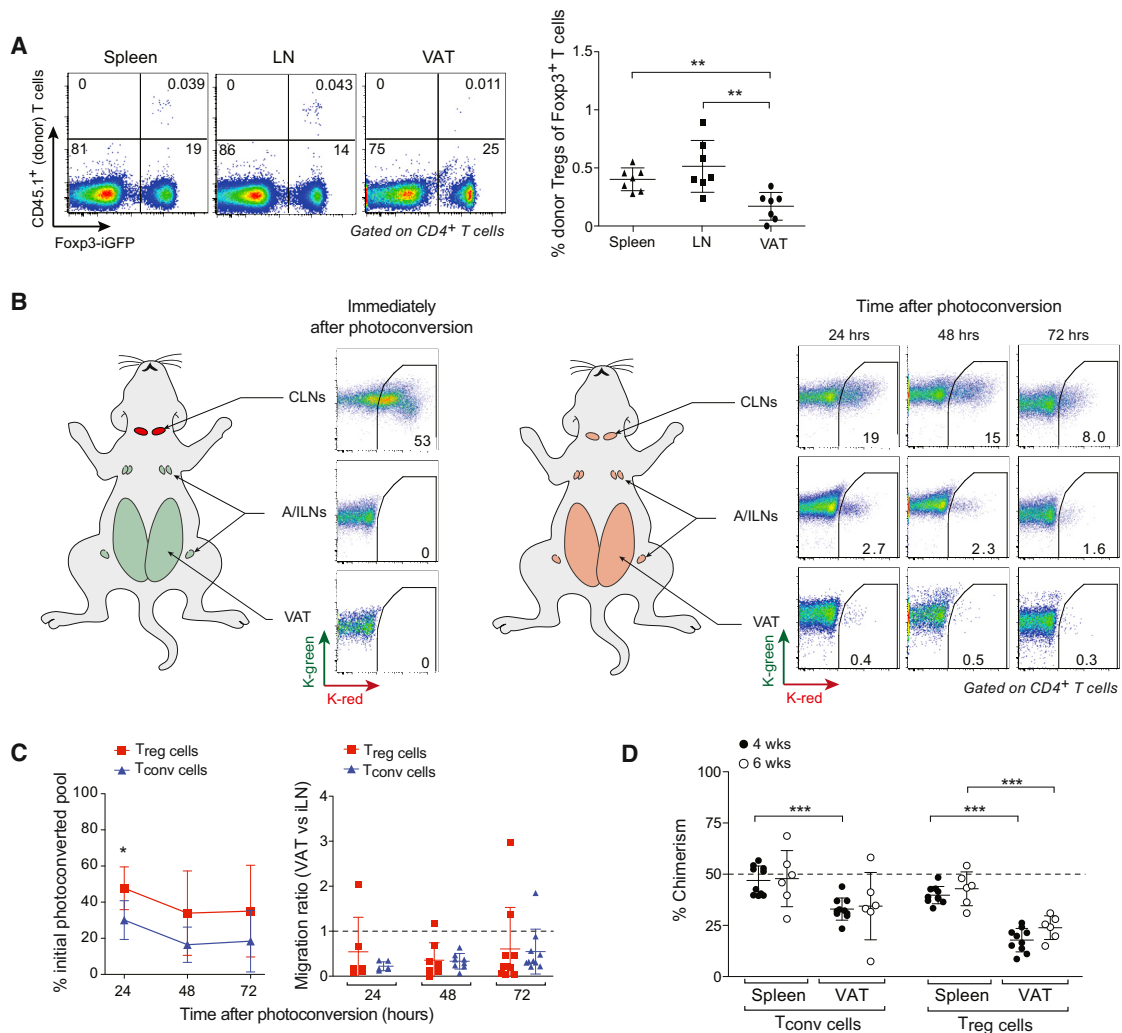


### Figure 2. Little Contribution of Circulating Tregs to the VAT Compartment of Lean Mice

(A) Transfer studies. Foxp3<sup>+</sup>CD4<sup>+</sup> Tregs were sorted from pooled spleen and LNs of CD45.1 Foxp3<sup>GFP</sup> donors and iv transferred into CD45.2 Foxp3<sup>GFP</sup> recipients, and organs were analyzed 4 weeks later. Left panels: representative flow cytometry plots; right panels: summary data pooled from three independent experiments.

(B) Photoconversion experiments. Experimental set-up and representative flow cytometry plots of CD4<sup>+</sup> T cells isolated from the designated tissues immediately after (left panels) and 24, 48, or 72 hr after (right panels) photoconversion. CLN, cervical lymph node. A/iLN, pooled axial and inguinal lymph nodes; VAT, visceral adipose tissue.

(C) Summary data for dynamics of the Kaede-red<sup>+</sup> population. Left panel: rate of egress of Treg and Tconv cells labeled in the CLNs; right panel: migration ratios of Treg and Tconv cells expressed as a ratio over the analogous populations migrating to A/iLNs.

(D) Parabiosis experiments. Chimerism of Tconv and Treg cells represented as the percent of donor-derived cells among total live cells of that type. For all panels data, are from two to three independent experiments. Mean  $\pm$  SD.

confirmed the similar behaviors of splenic and VAT Treg cells (Figure 3B). While substantially more Treg than Tconv cells were cycling in the spleen, the difference was less evident in VAT.

Cell turnover was examined by quantifying labeling by bromodeoxyuridine (BrdU), another nucleoside analog, during long-term incorporation and a subsequent chase. The rate and extent of BrdU labeling for spleen and VAT Treg cells were indistinguishable over the 5-week period of BrdU administration in the drinking water; these parameters were also similar for VAT Tconv cells (Figure 3C, left curves). However, the loss of BrdU labeling

over the 5-week time period subsequent to its removal from the drinking water revealed a substantially faster decay rate for splenic than for VAT Tregs: a half-life of 10.8 days in the former case and 24.5 days in the latter (Figure 3C, right curves). The VAT Tconv cell population showed a half-life of 16.5 days in the same experiment, indicating that slow turnover is not a characteristic of all T cell populations residing in this adipose tissue depot and explaining the rise in Treg percentage within the CD4<sup>+</sup> compartment over time.

The similarity in spleen and VAT Treg cycling rates might have masked clonal expansions in response to antigen(s). We

previously reported that the VAT, but not lymphoid tissue, Treg TCR repertoire included multiple repeats of particular  $\alpha$  and  $\beta$  chains, but these experiments employed a line of mice genetically engineered to minimize options for TCR variable (V) and joining (J) segment usage (Feuerer et al., 2009), meaning that we could not estimate the true frequency of TCR repeats. Here, individual Treg cells from LN or VAT and Tconv cells from VAT of >25-week-old B6 mice were sorted into 96-well plates, and the sequences of their TCR- $\beta$  and TCR- $\alpha$  complementarity-determining region(CDR)3s were determined. For both TCR chains, LN Tregs showed few CDR3 repeats (Figure 3D, left pies); the slight increase over the near-zero we previously reported (Feuerer et al., 2009; Burzyn et al., 2013) most likely reflects the advanced age of the mice in our current study. However, VAT Treg cells were very different: all mice showed numerous clonal expansions, rising to as high as ~80% of the sequences examined (Figure 3D, center pies). Each mouse harbored multiple expanded clones, none of which were common to different mice, and no clone was shared between VAT Treg cells and LN Treg or VAT Tconv cells. In contrast, VAT Tconv cells showed a degree of clonal expansion only slightly greater than that found for LN Tregs (Figure 3D, right pies). There was a linear relationship between the frequency of repeated CDR3s and the fraction of Tregs in the VAT CD4<sup>+</sup> T cell compartment (Figures 3E and 3F).

For both the TCR- $\alpha$  and - $\beta$  chains, CDR3 lengths were indistinguishable for the repeated VAT and the LN Treg populations (Figure 3G). Interestingly, N-nucleotide addition was reduced in repeated VAT Treg TCR- $\beta$ , but not TCR- $\alpha$ , chains—notably, a quarter of the clonally expanded Treg sequences had no N-nucleotides at all, and fewer of them had N-additions of >3 nucleotides (Figure 3H). This finding suggests that the corresponding cells differentiated around the time when terminal deoxynucleotidyl transferase (TdT) is usually turned on (i.e., within a week after birth) (Bogue et al., 1992). (Note that the TCR- $\alpha$  chain is usually rearranged days after the  $\beta$  chain.)

### Early Seeding of VAT Tregs

On the basis of the TCR sequencing results, we hypothesized that the VAT Treg compartment is seeded early on, in the first weeks of life, followed by an indolent expansion—of certain clones in particular. As a first test of this notion, we thymectomized or sham-operated B6 mice at 3 to 4 or 13.5 weeks of age (prior to or early during the typical expansion of the VAT Treg population, respectively), let them age until 25 weeks old (the usual peak of accumulation), and analyzed the Treg compartments by flow cytometry. There was no significant reduction in the fraction or number of Foxp3<sup>+</sup>CD4<sup>+</sup> Treg cells in VAT of thymectomized versus sham-operated animals, irrespective of the age at which surgery was performed (Figure 4A). Neither was there a detectable loss when we focused on bona fide VAT Treg cells expressing Gata3 (Figure 4B). Thus, thymic output beyond 3 weeks of age was not required for establishment of a robust VAT Treg compartment.

A complementary approach was to exploit B6.Foxp3<sup>DTR</sup> mice to systemically ablate Treg cells at different ages and then assess the degree to which the VAT Treg population could be reconstituted from newly generated cells. B6.Foxp3<sup>DTR</sup> mice of

various ages were depleted of Treg cells by two injections of diphtheria toxin 1 day apart, a regimen known to effectively deplete them without provoking autoimmune manifestations (Feuerer et al., 2009); they were then left until 25 weeks old, when reconstitution of the Treg compartments was assessed by flow cytometry. When Treg cells were punctually ablated at 16/17 days or 3 weeks of age, VAT Tregs attained a normal frequency and number by 25 weeks, if not slightly elevated ones (Figure 4C). In contrast, the VAT Treg compartment was compromised when punctual Treg ablation was performed later on, at 8 or 13 weeks of age. This finding was substantiated by focusing on Gata3<sup>+</sup> bona fide VAT Treg cells (Figure 4D). In contrast, splenic Treg populations in the same mice did not show any such deficiencies (Figure 4C).

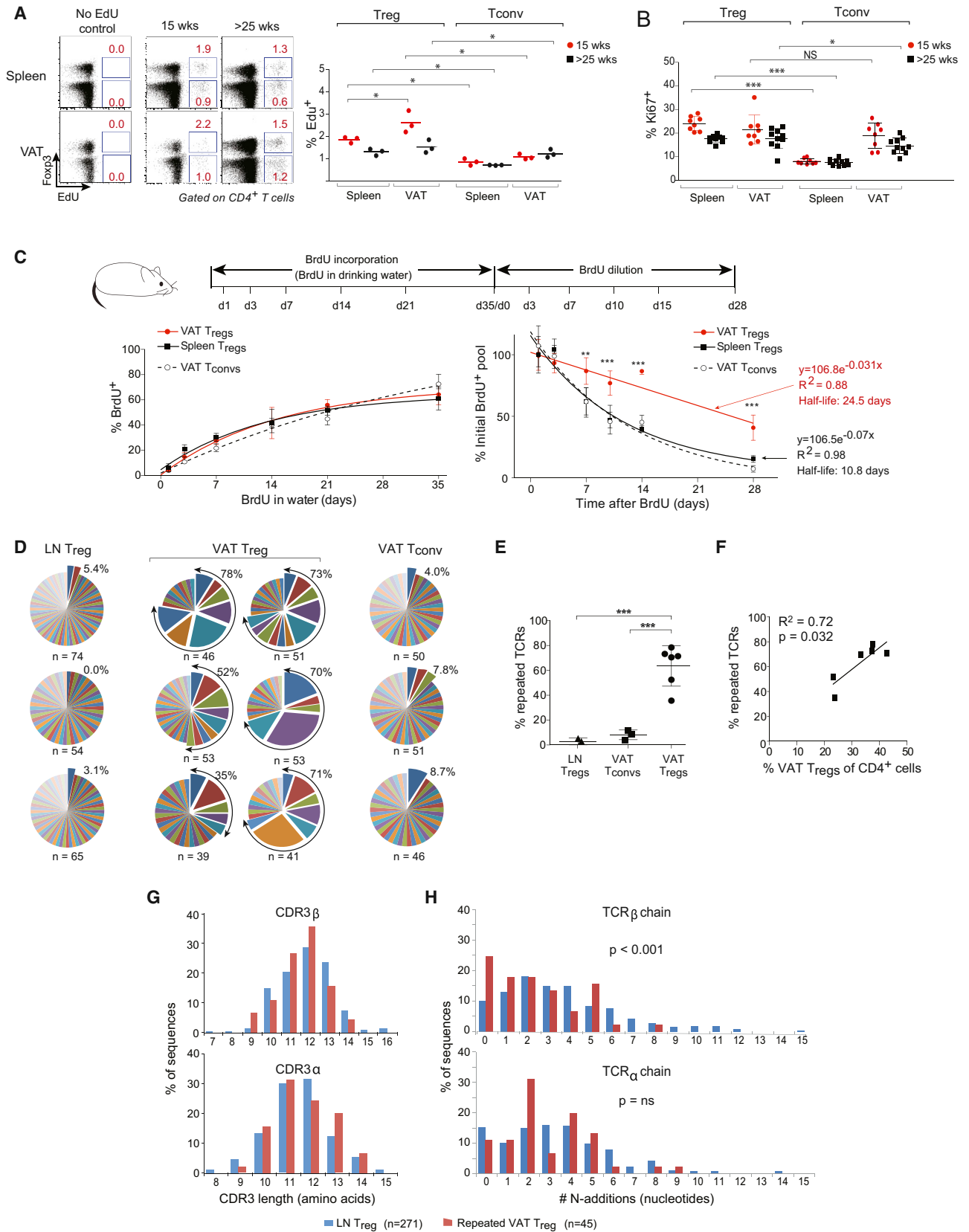
### VAT Treg Cells Depend on MHCII Molecules and Associate with Myeloid Cells Expressing Them

The ready detection of VAT Treg clonal expansion (Feuerer et al., 2009) (Figure 3D), coupled with the identification of TCRs with the same CDR3 protein sequence specified by different nucleotide sequences in mice with constrained TCR diversity (Feuerer et al., 2009), suggested that VAT Tregs might be responding to one or more adipose tissue antigens. Recognition of cognate antigen/major histocompatibility complex (Ag/MHC) molecules on the surface of local antigen-presenting cells (APCs) by T cells is usually the major driver of their retention in tissues. We therefore sought to identify the class of MHC molecules recognized by VAT Treg cells.

CD1d is a non-classical MHC-like molecule that specializes in presenting lipid antigens to subsets of CD4<sup>+</sup>, CD8<sup>+</sup>, and double-negative T cells (Adams and Luoma, 2013) and is, therefore, an interesting candidate for presentation of Ags capable of stimulating VAT Tregs, especially given that they can take up lipids through surface-bound CD36 (Cipolletta et al., 2012). However, we found that *Cd1d*-KO mice maintained on ND had a VAT Treg compartment of typical size expressing normal levels of Foxp3 (data not shown). (Conflicting data on this point appear in the literature, as summarized in Mathis [2013].)

The next most likely possibility was that, like standard Treg cells, VAT Tregs see Ag(s) in the context of MHC class-II (MHCII) molecules. As anticipated (Cosgrove et al., 1991), MHCII-deficient mice had reduced numbers of CD4<sup>+</sup> T lymphocytes in the spleen, both Tconv and Treg cells (Figure 5A, left panels). This dearth was true of VAT Treg cells as well (Figure 5A, middle panels), and few of the remaining VAT Tregs expressed Gata3 (Figure 5A, right panels). Thus, Treg cells residing in the visceral adipose depot are thymically selected and/or peripherally maintained by interactions with APCs displaying MHCII molecules.

To identify the relevant MHCII<sup>+</sup> APCs, we turned to flow cytometry and confocal microscopy. Cytofluorimetric analysis of VAT from >25-week-old B6 mice revealed all MHCII-expressing cells to be CD45<sup>+</sup> (i.e., of the hematopoietic lineage) (Figure 5B). (Note that in all of these analyses gates were rigorously set by comparison with data from MHCII-KO mice.) Co-staining for CD11b and CD11c split the CD45<sup>+</sup> population into five major subsets: I, CD11b<sup>+</sup>11c<sup>hi</sup> MFs; II, CD11b<sup>+</sup>11c<sup>lo</sup> MFs/monocytes; III, CD11b<sup>+</sup>11c<sup>-</sup> eosinophils; IV, CD11b<sup>-</sup>11c<sup>-</sup> lymphoid-type cells; and V, CD11b<sup>-</sup>11c<sup>+</sup> DCs (Figure 5C). All cells within



(legend on next page)

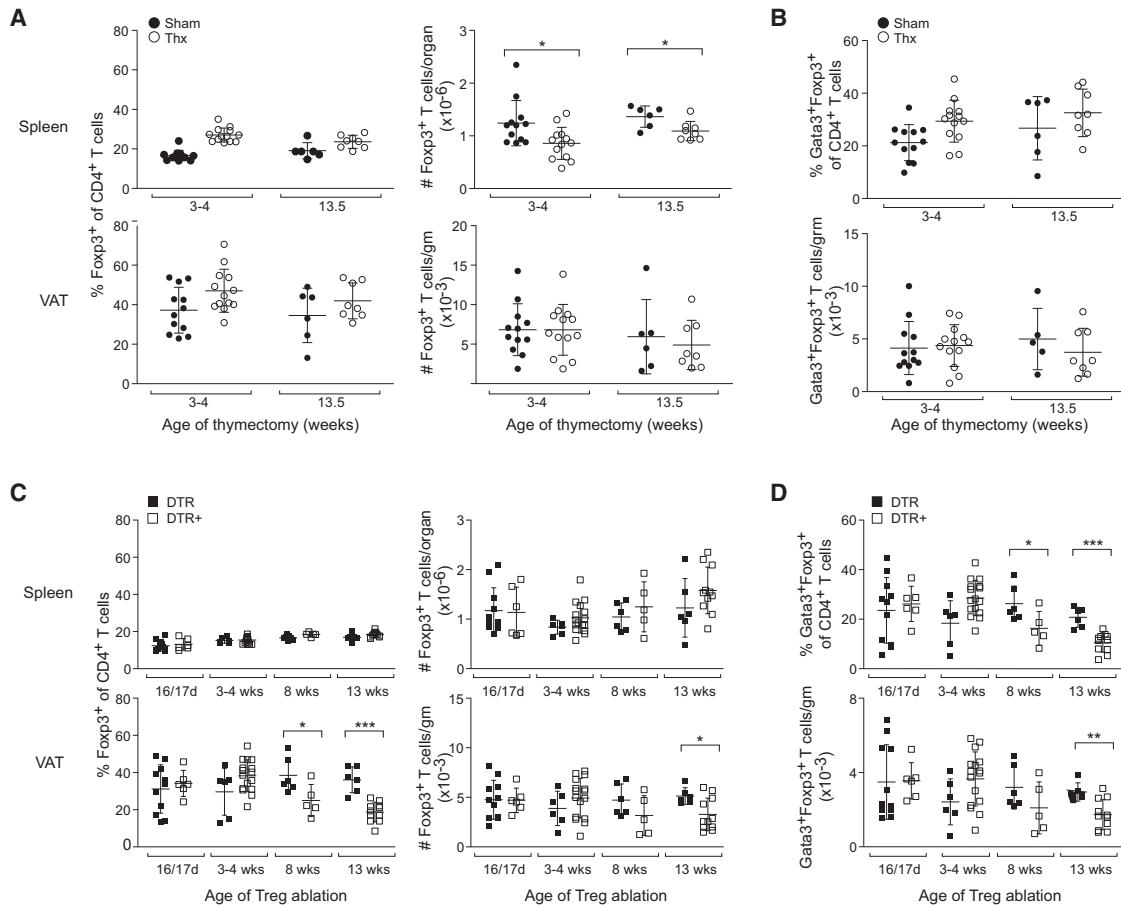


**Figure 4. Early Seeding of VAT Tregs from the Thymus**

(A and B) Thymectomy experiments.

(A) Frequencies (left) and numbers (right) of Foxp3<sup>+</sup> T cells in tissues of 25-week-old B6 mice thymectomized or sham operated.

(B) Frequencies (top) and numbers (bottom) of Gata3<sup>+</sup> Tregs in VAT.

(C and D) Punctual ablation of Tregs.

(C) Frequencies (left) and numbers (right) of Foxp3<sup>+</sup> T cells in tissues of 25-week-old B6.Foxp3<sup>DTR</sup> mice and their DTR<sup>-</sup> littermates after DT administration at the indicated ages.

(D) Frequencies (top) and numbers (bottom) of Gata3<sup>+</sup> Tregs in VAT. All experiments: pooled data from two to three independent experiments. Error bars indicate mean  $\pm$  SD.

population V, most within populations I and II, and a few within population IV expressed MHCII molecules. The MHCII-expressing cells within gate IV were B cells (Figure S2).

These findings fit very well with observations made using confocal microscopy and histocytometry. Confocal analysis revealed numerous irregularly shaped MHCII-positive APCs

**Figure 3. Micro-Expansions of VAT Treg Clones**

(A) Degree of VAT Treg proliferation at steady state. 15- or 30-week-old B6 mice were pulsed for 4 hr with EdU, at which time tissues were analyzed for incorporation. Left: representative flow cytometry plots; right: summary data.

(B) VAT Treg cells in cycle. Summary data for Ki67 expression by T cell subsets of 15- or 30-week-old mice.

(C) Long-term VAT Treg proliferation and turnover. Top: schematic representation of BrdU pulse/chase experiment. 15-week-old B6 mice were given BrdU in the drinking water according to the protocol illustrated; BrdU incorporation was assessed by flow cytometry. Bottom left: quantification of BrdU incorporation by Treg or Tconv cells of mice analyzed on the indicated days after introducing BrdU in the drinking water. Bottom right: same for mice analyzed on the indicated days after removal of BrdU from the drinking water, expressed as percent of the starting BrdU<sup>+</sup>Foxp3<sup>+</sup> Treg pool on day 0 of chase. An exponential decay line was fitted to each data set; corresponding equations, R<sup>2</sup> values, and half-lives are presented. n = 5–7 for each time-point; pooled data from three independent experiments.

(D) TCR CDR3 $\alpha$  and CDR3 $\beta$  sequences for various T cell compartments. Each pie chart represents a single mouse, and the width of the slice illustrates the frequency of a clone's repeats. Total frequency of expanded clones is shown at the top right.

(E) Quantification of clonal TCR frequencies. Sequences obtained from three to six individual mice for each compartment.

(F) Correlation between frequency of Foxp3<sup>+</sup> Tregs and total frequency of repeated TCRs in each individual. R<sup>2</sup> and p values generated using linear regression.

(G) Length of TCR CDR3 $\alpha$  and - $\beta$  amino-acid sequences.

(H) Length of TCR N-region nucleotide sequences. Error bars indicate mean  $\pm$  SD.

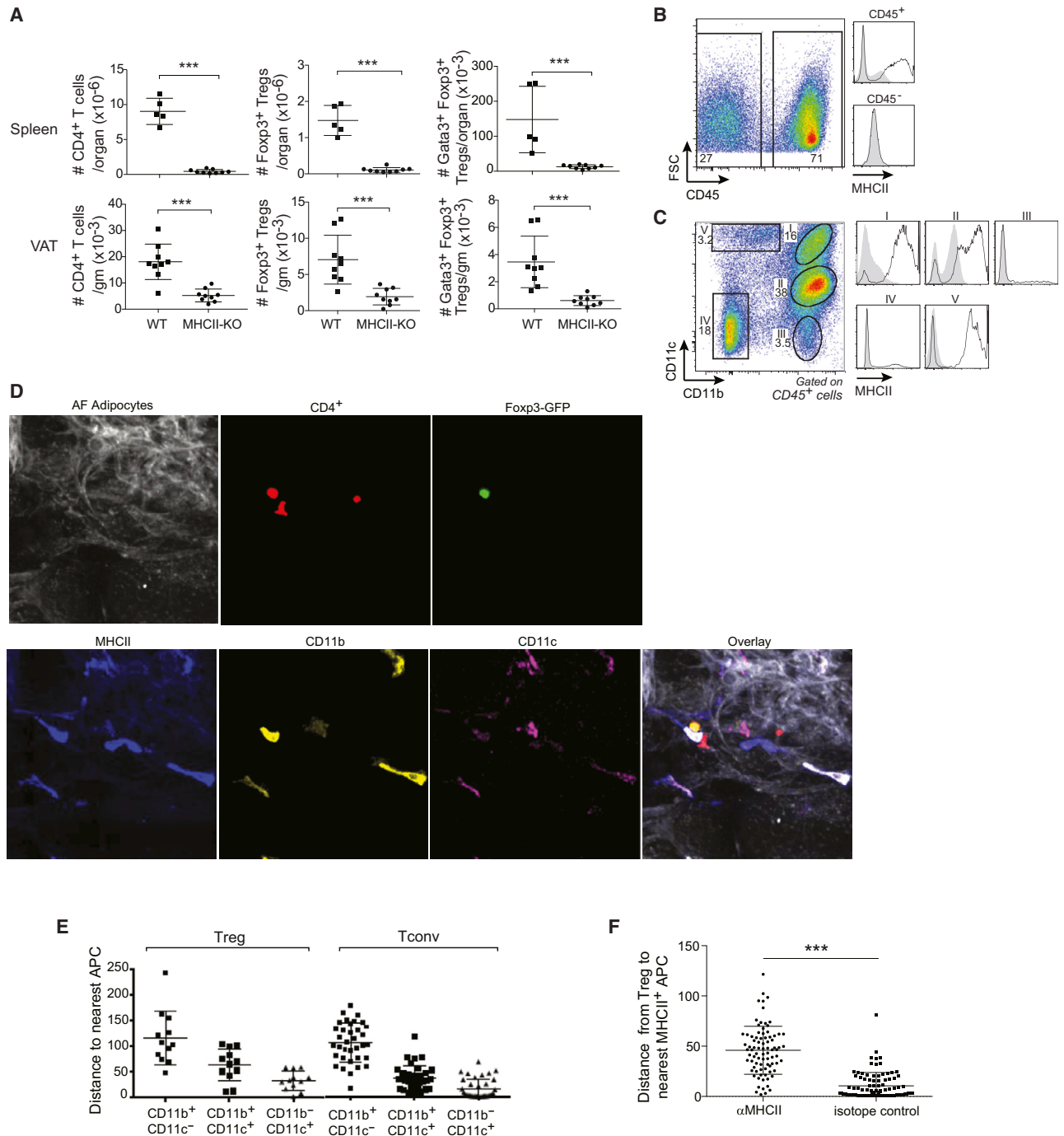


**Figure 5. VAT Treg Dependence on MHCII Molecules**

(A) Summary data for Foxp3 and Gata3 expression by CD4<sup>+</sup> T cells in tissues of 20-week-old MHCII-KO mice and their WT littermates.

(B and C) Flow cytometry on VAT MHCII-expressing cells.

(B) Expression by immune (CD45<sup>+</sup>) versus non-immune (CD45<sup>-</sup>) cells in VAT of >20-week-old MHCII-KO mice (gray shading) and their WT littermates (black line).

(C) By CD11b/c splits of VAT CD45<sup>+</sup> cells. Same mice as in (B). To the left of each panel are histograms of MHCII molecule expression by the subsets delineated on the dot plot. (CI), CD11b<sup>+</sup>c<sup>hi</sup> MFs (confirmed as F480<sup>+</sup>); (CII), CD11b<sup>+</sup>c<sup>lo</sup> MFs and monocytes (the latter confirmed as Ly6c<sup>+</sup> and F480<sup>+</sup>); (CIII), CD11b<sup>+</sup>c<sup>-</sup> eosinophils (confirmed as Siglec-F<sup>+</sup>); (CIV), CD11b<sup>-</sup>c<sup>-</sup> lymphocytes, NK cells and ILCs (see [C]); (CV), CD11b<sup>-</sup>c<sup>+</sup> DCs (confirmed as F480<sup>-</sup>).

(D) VAT was obtained from 16-week-old B6 mice, and whole-mount tissues were stained for CD4 (red), MHCII (blue), CD11b (yellow), and CD11c (purple); Foxp3 expression detected by measuring GFP expression (green); VAT morphology determined via autofluorescence (white). See a second example in Figure S3C.

(E) Foxp3<sup>+</sup>CD4<sup>+</sup> Treg and Foxp3<sup>-</sup>CD4<sup>+</sup> Tconv cells were distinguished by histocytometry, as were the indicated CD11b/c splits of APCs.

(F) Similar measurements for Treg proximity to MHCII<sup>+</sup> cells (intracellular staining) in mice treated twice, 3 days apart, with anti-MHCII mAb and examined 6 hr after the second shot. Data pooled from two to three independent experiments in all cases. Error bars indicate mean ± SD.

scattered throughout VAT, many with a classical dendritic morphology, while there was no clear expression of MHCII molecules by adipocytes; less frequent Foxp3<sup>-</sup>CD4<sup>+</sup> and rare Foxp3<sup>+</sup>CD4<sup>+</sup> T cells were also dispersed through the adipose tissue (Figures S3A and S3B). Higher magnification demonstrated close association between MHCII<sup>+</sup> APCs and certain, but not all, of the Tconv and Treg cells—sometimes the two types of T cell were in contact with the same APC (insets of Figures S3A and S3B). Next, we measured the distance between individual CD4<sup>+</sup> T cells and the closest APC, distinguishing between Foxp3<sup>+</sup> and Foxp3<sup>-</sup> T cells, and delineating APC subsets according to histocytometry of CD11b and CD11c expression (Figures S4, 5D and S3C). Treg and Tconv cells could both be found in close contact with CD11b<sup>+</sup>c<sup>+</sup> MFs and CD11b<sup>-</sup>c<sup>+</sup> DCs, although in both cases the association with DCs was closest (Figure 5E). The relevance of these interactions was established by their significant reduction in mice treated with an anti-MHCII mAb for 3 days before sacrifice (Figure 5F).

### IL-33 Promotion of VAT Treg Accumulation

The *Il1r1* gene, which encodes ST2, the receptor for the cytokine interleukin (IL)-33 has a pattern of expression by VAT Treg cells that parallels that of *Pparg* (Cipolletta et al., 2012). In addition, administration of IL-33 to obese mice was reported to improve both adipose tissue inflammation and systemic insulin resistance, attributed at that time to this cytokine's ability to promote polarization of MFs to an M2-like phenotype and to foster the differentiation of Th2 cells (Miller et al., 2010). But IL-33 is also known to serve as a T-cell-inciting alarmin (Bonilla et al., 2012); so, given its documented expression by adipocytes (Wood et al., 2009), we hypothesized that Treg cells might accumulate in VAT in response to IL-33 expression.

Cytofluorometric analysis showed that ST2<sup>+</sup> Treg cells were barely detectable in the spleen at all ages examined (Figures 6A, upper panels, and 6B). Many more visceral-adipose Tregs displayed ST2, their fractional representation rising with age to attain close to 90% of VAT Tregs in B6 mice >25 weeks of age (Figures 6A, lower panels, and 6B). Interestingly, this enrichment for ST2<sup>+</sup> Tregs in VAT depended at least to some degree on PPAR $\gamma$ , as it was less evident in mice bearing a *Pparg* null mutation specifically in Tregs (Figure 6C).

Since IL-33 is an alarmin, we wondered how its expression in VAT related to the high number of ST2<sup>+</sup> Tregs in VAT. PCR quantification revealed similar levels of *Il33* transcripts in whole-adipose and spleen tissue of 4- to 6-week-old mice (Figure 6D). Levels increased significantly in both tissues at 8–10 weeks of age, when expansion of the VAT Treg population usually begins in our colony, but decreased over time in adipose tissue. *Il33* transcript levels in VAT and spleen were neither unusually high (note lung levels) nor unusually low (note muscle levels) (Figure 6D).

As it was difficult to visualize IL-33 expression by flow cytometry, we turned to immunohistology to establish which VAT cells expressed this cytokine. In 24-week-old (unmanipulated) B6 mice, cells expressing IL-33, mostly in the nucleus, were located primarily at the edges of the visceral adipose mass (Figure 6E). By far, most of these cells were neither hematopoietic nor endothelial as they did not, except in rare cases, display either CD45 or CD31 (Figures S5A and S5B); neither did they stain for smooth

muscle actin, which is expressed by some fibroblasts (as well as other cell lineages) (not shown). However, many of the IL-33-expressing cells did express cadherin-11 (Figure 6F), suggesting that they were related to fibroblast reticular cells (Malhotra et al., 2012). We did not detect any clear differences in mice of ages ranging from 4 to 24 weeks (not shown).

To assess the role of IL-33/ST2 in VAT Treg cell accumulation in lean mice, we performed loss- and gain-of-function experiments. 25-week-old B6 mice lacking ST2 had a reduced fraction and number of VAT, but not splenic, Tregs (Figure 7A). This difference was even more significant when we focused on bona fide VAT Tregs expressing Gata3 (Figure 7B). Conversely, two injections of IL-33 into 8-week-old wild-type (WT) B6 mice provoked an impressive expansion of the VAT Treg population, as their numbers/gm tissue increased more than an order of magnitude in just 7 days (Figure 7C, lower panel). The expanded Treg population was enriched in cells expressing both ST2 and Gata3 (Figure 7D, lower panel), and the majority of ST2 expressers were in cycle, evidenced by co-expression of Ki67 (Figure 7E, lower panel). The Treg population in the spleen also expanded in response to IL-33—and expressed ST2, Gata3, and Ki67 more often than splenic Tregs from PBS-injected littermates did—but the differences were far less striking than for VAT Tregs (Figures 7C–7E, upper panels). Similarly, IL-33 had a relatively minor effect on Tregs in subcutaneous adipose tissue, the inguinal depot (Figure S6).

That most ST2<sup>+</sup> Tregs in the adipose compartment (>75%) were in cycle argued for population expansion as a major contributor at this stage, rather than influx of cells from other organs. The expansion abated over time, although a significantly elevated fraction and number of VAT Tregs was still evident 4 weeks after IL-33 injection (Figure 7F). Interestingly, IL-33 induction of Treg expression in neither the spleen nor VAT depended on TCR-Ag/MHCII interactions as anti-MHCII mAb blockade had no detectable effect (Figure 7G).

## DISCUSSION

The overall goal of this series of experiments was to elucidate the means by which Treg cells accumulate in VAT as lean mice age. Our results argue that the VAT Treg compartment is seeded from thymocytes generated during the first weeks of life and noticeably expands after week 10 as a result of indolent Treg proliferation, of certain clones in particular, coupled with enhanced survival. Here, we have identified Ag/MHCII and IL-33 as drivers of VAT Treg accumulation in lean mice. We previously reported that PPAR $\gamma$  agonists promote VAT Treg survival in the lean state (Cipolletta et al., 2012). How do these various factors interplay?

### Ag/MHC: Retaining Tregs within VAT

Retention of T cells within non-lymphoid tissues generally depends on local recognition of cognate Ag presented by MHC molecules displayed on the surface of APCs. That Tregs were retained in epididymal adipose tissue through recognition of cognate Ag/MHC molecules was indicated by their striking clonal expansion at that site in mice with a normal repertoire of TCRs (Figure 3), as well as by our prior documentation of multiple clones with the same CDR3- $\alpha$  amino acid sequence specified by

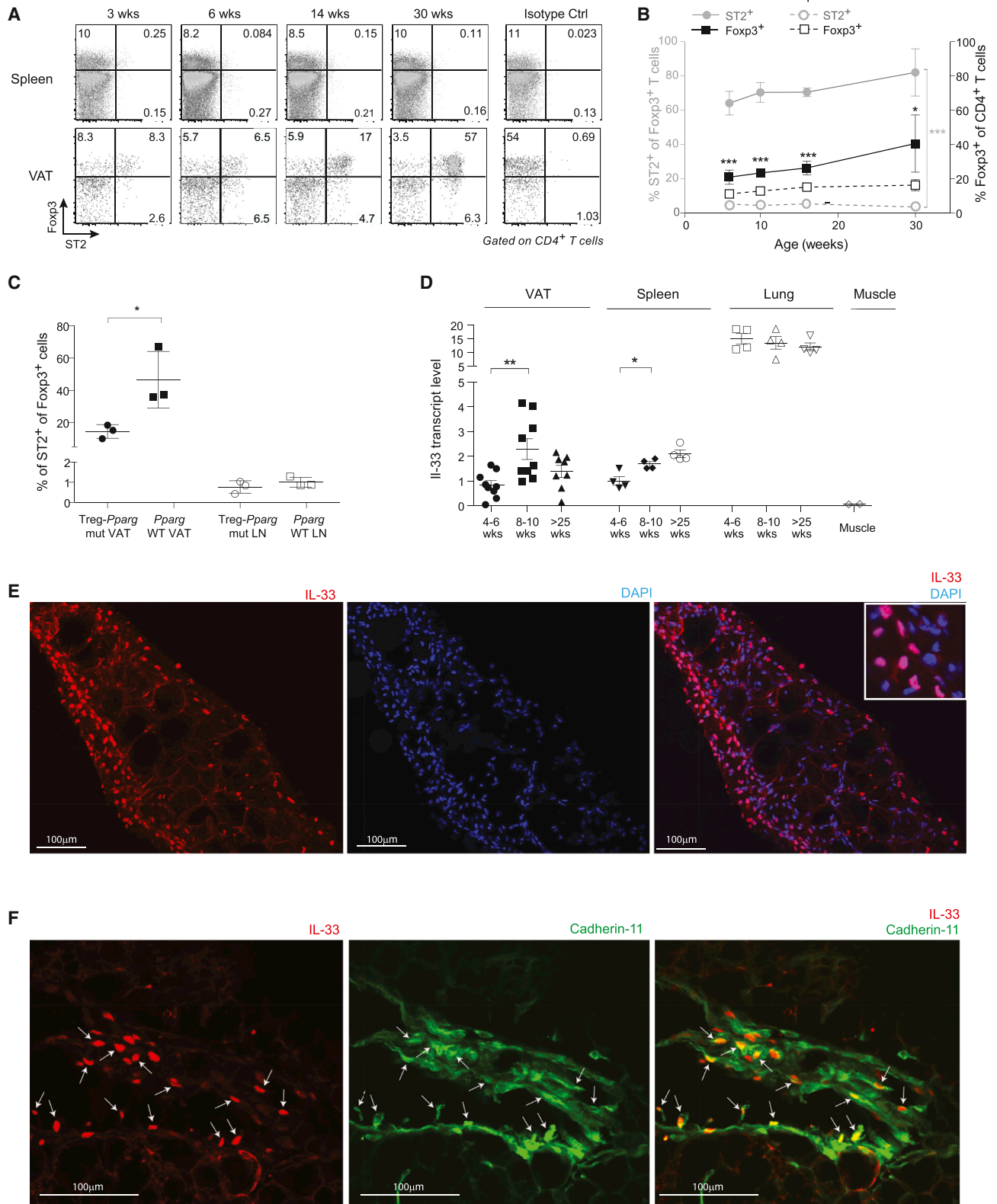


**Figure 6. ST2 and IL-33 Expression in VAT**

(A–C) ST2 expression.

(A) Representative cytofluorimetric dot plots of ST2 expression in Tregs of B6. Numbers refer to % CD4<sup>+</sup> cells.

(legend continued on next page)

different nucleotide sequences in mice with an artificially restricted TCR repertoire (Feuerer et al., 2009).

The relevant class of MHC molecules was MHCII, specifically the A $\alpha$ B $\beta$  dimer, given that E $\alpha$ E $\beta$  is absent from B6 mice. Indeed, we found a preponderance of MHCII<sup>+</sup> CD11b<sup>+</sup>c<sup>+</sup> MFs and some MHCII<sup>+</sup> CD11b<sup>-</sup>c<sup>+</sup> DCs in epididymal adipose tissue and observed Tregs in close association with both subsets, which was dependent on expression of MHCII molecules. Our findings are consistent with a report highlighting the importance of MHCII<sup>+</sup> MFs in the stimulation of VAT Tconv cells (Morris et al., 2013), but do not support previous contentions that MHCII molecule expression on adipocytes is key to VAT Tconv cell activation (Deng et al., 2013). We did not expressly examine expression of MHCII molecules on innate lymphoid cells (ILCs) in VAT, a cell-type reported to display these molecules in other contexts, but given the few MHCII<sup>+</sup> cells falling within the relevant gate (Figure S2), they would have to be rare, at least in aging lean mice. The identity of the culprit Ag(s) is unknown at this time.

#### PPAR $\gamma$ : Molding the Treg Phenotype for Survival in VAT

We previously established that the accumulation and phenotype of VAT Treg cells depend critically on PPAR $\gamma$ , the “master regulator” of adipocyte differentiation and function (Cipolletta et al., 2012). Retroviral transduction experiments showed that PPAR $\gamma$  controls expression of the transcripts distinguishing adipose tissue from lymphoid-organ Tregs, notably a set of transcripts encoding proteins involved in lipid metabolism and likely critical for Treg survival in a lipid-rich environment. Indeed, injection of a PPAR $\gamma$  antagonist into lean mice provoked rapid disintegration of the VAT Treg phenotype, compromising their survival (Cipolletta et al., 2012).

We do not know yet whether VAT Tregs emerge from the thymus with their characteristic transcriptome already fixed or, alternatively, whether they arrive in the adipose tissue looking and acting like lymphoid tissue Tregs and eventually adopt a bona fide VAT Treg phenotype in response to local cues. The absence of anti-PPAR $\gamma$  mAbs compatible with cytofluorometric analysis renders this issue difficult to address at present. However, we suspect that the answer lies somewhere between these two possibilities. We do detect *Pparg* gene transcripts at low levels in the circulating Tregs of lymphoid organs; so it is possible that a PPAR $\gamma$ -expressing VAT Treg precursor is generated in the thymus, either a rare one expressing low levels of PPAR $\gamma$  or an extremely rare one making substantial levels. The precursor could emerge from the thymus; circulate through the lymphoid organs; and, eventually, if it expresses the correct TCR, be retained in VAT, where PPAR $\gamma$  ligands and other local mediators could confirm and lock in the VAT Treg phenotype.

#### IL-33: Expanding the VAT Treg Compartment with Aging

IL-33, a member of the IL-1 family of cytokines, is garnering more and more attention (Garlanda et al., 2013). Secreted mostly by stromal and parenchymal cells, such as epithelial and endothelial cells, it is best known for promoting type-2 immunity through actions on type-2 ILCs, T helper (Th)2 cells, and anti-inflammatory MFs. It can also act as an alarmin, released by necrotic cells to report on recent or impending tissue damage (e.g., hypoxia or mechanical stress). Most recently, attention has turned to IL-33's ability to expand Treg populations, both in lymphoid organs (Turnquist et al., 2011; Schiering et al., 2014) and in the colonic lamina propria (Schiering et al., 2014).

IL-33 and its receptor ST2 were found to be expressed in human adipose tissue (Wood et al., 2009). Moreover, injection of IL-33 into HFD-fed mice reduced adiposity, inflammation, and insulin resistance (Miller et al., 2010). These effects were attributed to IL-33's ability to promote Th2 responses and polarization of MFs toward an anti-inflammatory phenotype. However, interpretation of these findings was confounded by the influence of IL-33 on adiposity under the long-term experimental conditions employed, raising the question of whether the effects on inflammation might only be secondary. A later study on the impact of IL-33 in VAT highlighted a pathway encompassing ILCs, eosinophils, and anti-inflammatory MFs (Molofsky et al., 2013).

Given the above-cited results and the fact that *Il1r1* transcripts were among those most differentially expressed in VAT versus lymphoid tissue Tregs (Cipolletta et al., 2012), we explored the hypothesis that IL-33 might be an important driver of Treg accumulation in the epididymal depot of aging lean mice. Results from both gain- and loss-of-function experiments supported this notion. While, under our conditions, IL-33 injection expanded the Treg compartments in both lymphoid tissues (as anticipated from published data (Turnquist et al., 2011; Schiering et al., 2014) and VAT (without significantly impacting body or fat weight), the increase was more than an order of magnitude greater at the adipose site. This was a long-lasting effect as even a month after IL-33 injection VAT Tregs were significantly over-represented. The fraction of VAT Tregs expressing ST2 was impressively high, although, per gram tissue, VAT expressed IL-33 transcripts at levels quite similar to those of spleen. It is possible that the form of IL-33 differs at the two sites: nuclear versus secreted, differentially cleaved or otherwise post-translationally modified, bound to soluble ST2 or not, etc. Or it may be that the greater response of VAT Tregs reflects aspects of their distinct phenotype; for example, their frequent expression of ST2. The latter explanation seems more easy to reconcile with the fact that a striking adipose:lymphoid tissue differential is seen after injection of IL-33 exogenously.

(B) Quantification of percent Tregs (right y axis) and percent Tregs displaying ST2 (left y axis). n = 4–9 for each age; data pooled from two independent experiments.

(C) Summary data on Treg expression of ST2 in VAT and LN of 20-week-old mice lacking PPAR $\gamma$  specifically on Tregs (Treg-*Pparg* mut) and their WT littermates. (D–F) IL-33 expression.

(D) PCR quantification of IL-33 transcript levels for various tissues from mice of diverse ages.

(E) Immunohistology on VAT tissue of 24-week-old B6 mice stained for IL-33 or/and by DAPI, Magnification, 20 $\times$ . Higher-magnification (60 $\times$ ) inset in the right panel illustrates nuclear staining of IL-33.

(F) Immunohistology on the same tissues, stained for IL-33 or/and Cadherin-11. Magnification = 40 $\times$ . Arrows indicate doubly stained cells. Error bars indicate mean  $\pm$  SD.

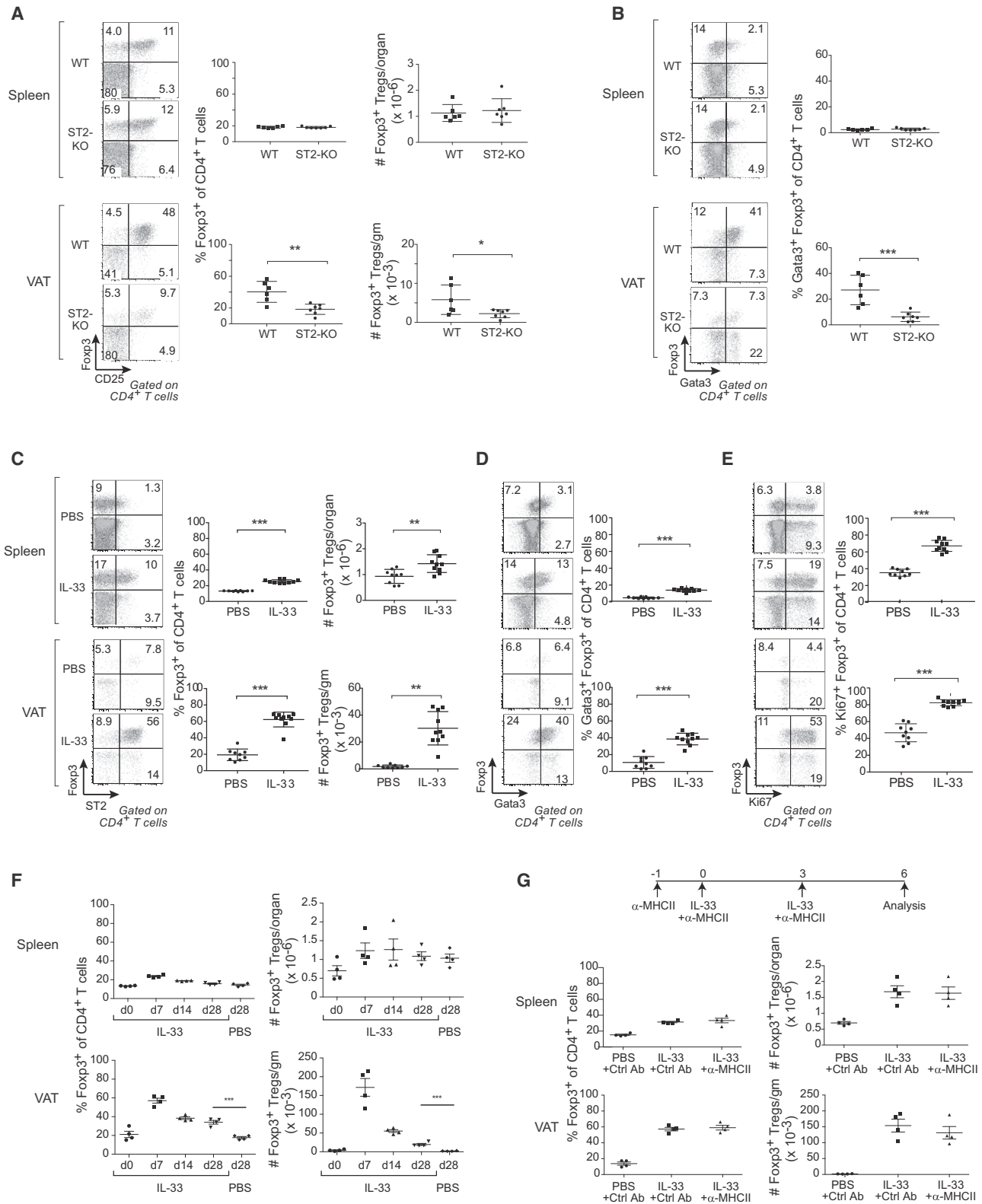


**Figure 7. IL-33 Promotion of VAT Treg Accumulation**

(A and B) Loss-of-function: ST2-KO.

(A) Representative dot plots (left panels) and summary quantification of frequencies (center panels) and numbers (right panels) of Fcpx3<sup>+</sup> Tregs in 25-week-old ST2-KO and -WT littermates.

(legend continued on next page)

At present, we cannot say to what extent the effects of increasing or decreasing ST2 signaling on the VAT Treg compartment are direct or require additional “helper” leukocyte populations. We can, however, say that the phenotype of the Tregs expanded in epididymal adipose tissue by IL-33 injection is typical of VAT Tregs. Interestingly, *Il1rl1* is a member of a cluster of genes co-regulated with *Pparg* in a set of metabolically relevant Treg data sets (Cipolletta et al., 2012), the VAT Treg population is reduced in mice lacking PPAR $\gamma$  specifically in Tregs (Cipolletta et al., 2012), and few of the remaining ones express St2 on their surface (Figure 6C), together suggesting a link between these two receptor pathways. Thus, as bona fide VAT Tregs emerge in adipose tissue, they may be sensitive to IL-33, whose concentration and/or form may respond to stress signals in the expanding fat pad (e.g., hypoxia or mechanical stretching).

This study has focused on factors driving accumulation of the unique Treg compartment in VAT of lean mice as they age. How these factors are inhibited or evaded in the development of obesity-induced inflammation and metabolic dysregulation is an important topic for future studies. Learning how these factors operate and interplay might expand therapeutic options for addressing the growing world-wide problem of metabolic irregularities.

## EXPERIMENTAL PROCEDURES

### Mice

Males of the specified ages were employed, all bred in our specific-pathogen-free facilities at Harvard Medical School. Experiments were conducted according to protocols approved by Harvard Medical School’s Institutional Animal Care and Use Committee (HMS protocol #02954). Details concerning the various mouse lines used and their breeding can be found in the [Supplemental Experimental Procedures](#).

### Mouse Manipulations

Details of cell isolation and flow cytometry can be found in the [Supplemental Experimental Procedures](#). For the Treg conversion and migration studies,  $5 \times 10^6$  Foxp3<sup>-</sup>CD4<sup>+</sup> Tconv cells or  $1 \times 10^6$  Foxp3<sup>+</sup>CD4<sup>+</sup> Treg cells were sorted from pooled spleen and LNs of 6- to 8-week-old CD45.1 Foxp3<sup>GFP</sup> donor mice, and were iv transferred into 20-week-old Foxp3<sup>GFP</sup>CD45.2 recipient mice. Recipients were sacrificed 4 weeks after transfer; LNs, spleen, and epididymal fat pads were removed, dispersed, and analyzed by flow cytometry.

Photoconversion of CLN cells in Kaede/B6 mice was performed as previously described (Morton et al., 2014). Briefly, 16- or 24-week-old Kaede/B6 mice were anesthetized with ketamine/xylazine in combination (10 mg/kg/2 mg/kg ip). The fur attached to the skin covering the CLNs was removed using depilatory cream, applied for 2 min. Mice were placed on their back, with an aluminum foil blanket covering all but the depilated area, and violet light (Electra Pro Series 405 nm Violet Handheld Laser, Laserglow Technologies) was shone onto the exposed area for a period of 3.5 min, the pre-established time for effective but innocuous photoconversion at this anatomical site. In order to manipulate the size of the light field (beam diameter: 3.5 mm) so that both CLNs could be exposed, we attached a lens to the laser to de-focus

the beam, and the source of the de-focused light beam was positioned 28 cm above the mouse.

Parabiotic pairs were generated as previously described (Wagers et al., 2002) by joining male mice from CD45.1 versus CD45.2 congenic strains. Matched male 8-week-old CD45.1 and CD45.2 congenic mice were anesthetized with 2.5% avertin (15  $\mu$ l per g of body weight) and were shaved along opposite lateral flanks. Skin was wiped with alcohol prep pads and further cleaned with Betadine solution and 70% isopropyl alcohol. Mirrored incisions were made on lateral aspects of the two mice, and sutures were placed through the olecranon and knee joints to secure the legs. Ventral and dorsal skin flaps were then approximated by staples and suture to conjoin the mice. Mice were taken 4 or 6 weeks after conjoinment for flow cytometric analysis of chimerism of different lymphoid cell compartments using CD45.1 versus CD45.2 distinction.

For monitoring of cell division and turnover, 1 mg EdU was iv injected into 15- or >25-week-old B6 mice, and 4 hr later, cells were processed for detection by the Click-iT EdU kit following the manufacturer’s (Molecular Probes) instructions. BrdU powder (Sigma) was added to the drinking water (0.8 mg/ml) and protected from the light; BrdU-containing water was changed every 2 days. Cells were processed for analysis and stained for BrdU detection at various times following the manufacturer’s instructions (BD Biosciences). A more precise protocol can be found in [Figure 3C](#) and its legend.

For thymectomies, mice of the designated ages were anesthetized with ketamine/xylazine in combination (10 mg/kg/2 mg/kg ip). The fur attached to the skin covering the thymus was removed using depilatory cream, applied for 2 min. An incision was made cutting the first three ribs, and the thymus was excised using forceps. The skin was closed and secured with two to three surgical clips.

For ablating Tregs, Foxp3<sup>DTR</sup> mice and DTR-negative littermates of the designated ages were ip injected with DT (Sigma) at 10 ng/g body weight for 2 consecutive days. Mice were aged to 25 weeks old, and lymphoid organs and VAT were analyzed by flow cytometry.

To expand Tregs, mice were ip injected with recombinant IL-33 (Biolegend) at 2  $\mu$ g per injection every 3 days for one week prior to analysis. In some experiments, MHCII molecules were blocked by ip injection of the mAb M5/114 (Bio-XCell), as per the scheme in [Figure 7G](#).

### TCR Analysis

Single Treg or Tconv cells were sorted from VAT or LN into 96-well plates. CDR3 $\alpha$  and  $\beta$  sequences were obtained using primer mixes covering all known chains. Extreme care was taken to avoid contamination. See further details in the [Supplemental Experimental Procedures](#).

### Imaging of VAT Cells and Histology of IL-33 Producers

VAT was isolated and fixed with 0.05 M phosphate buffer containing 0.1 M L-lysine, 2 mg/ml NaIO<sub>4</sub>, and 10 mg/ml paraformaldehyde for 18 hr at 4°C and was then equilibrated in 30% sucrose solution overnight. Tissues were frozen in OCT and stored at –80°C. Whole-mount tissue samples were then blocked for 4 hr in phosphate buffer with 1% normal mouse serum, 1% bovine serum albumin, and 0.3% Triton X-100. Tissues were stained for 18 hr at 4°C in the presence of CD11b-BV420, F4-80eF450 (eBioscience), CD4-BV510, Foxp3-GFP, CD3-PE, CD11c-AF647, and MHCII-AF700. Imaging was conducted on a Leica SP8 confocal microscope with a motorized stage for image tiling, equipped with a 1.2 NA 40 $\times$  oil emersion objective, with an additional optical zoom of 1.5 $\times$ . Tiled images composed of 5  $\times$  5 z stacks of 30–50  $\mu$ m each were compiled and used for final imaging analysis. Histocytometric subset identification was performed using the Imaris (Bitplane) surface creation utility. T cells were identified as CD3<sup>+</sup>MHCII<sup>–</sup>, and APCs were identified as CD3<sup>–</sup>MHCII<sup>+</sup>. Cells were

(B) Same except frequencies of Gata3<sup>+</sup>Foxp3<sup>+</sup> T cells within the CD4<sup>+</sup> compartment were examined.

(C–G) Gain-of-function: IL-33 administration.

(C and D) As per (A) except 8-week-old B6 mice were ip injected with 2  $\mu$ g of IL-33 twice, 3 days apart, and were analyzed 3 days later.

(E) T cells from the same mice were stained for Ki67. Left: representative dot plots; right: summary data.

(F) Mice treated with IL-33 as per (C) but were followed for longer times. Fraction (left) and number (right) of Tregs in spleen (top) or VAT (bottom).

(G) Mice treated with IL-33 and anti-MHCII mAb and analyzed as schematized. Fraction (left) and number (right) of Tregs in spleen (top) and VAT (bottom). Pooled from at least two independent experiments. Error bars indicate mean  $\pm$  SD.

then further subsetted by expression of CD4 and Foxp3 for T cells and CD11b, CD11c, and F4-80 for APCs. A more in-depth description of the histocytometric technique can be found in [Gerner et al. \(2012\)](#).

For IL-33 staining, VAT tissues were fixed and frozen in OCT as described above and then sectioned at a thickness of 50  $\mu$ m. Tissues were then permeabilized with 0.3% Triton X-100 in PBS for 5 min and blocked with 5% fetal bovine serum and 10% donkey serum in PBS at room temperature for 1 hr. Tissues were stained for 2 hr at room temperature in the presence of goat anti-IL-33 (R&D) and mouse anti-Cadherin 11 (Invitrogen), followed by staining for 1 hr at room temperature with Cy3-donkey anti-goat secondary antibody, Cy5-donkey anti-mouse secondary antibody (Jackson Laboratory), CD45-APC, CD31-Alexa Fluor 647 (Biolegend), or anti-SMA-FITC (Sigma-Aldrich). Tissue sections were further stained with DAPI for 5 min before imaging. Imaging was conducted on an Olympus FluoView confocal microscope with 20 $\times$  and 40 $\times$  objectives.

### Statistical Analyses

Data were routinely presented as mean  $\pm$  SD. Unless stated otherwise: significance was assessed by the Student's *t* test or ANOVA using Prism 5 (GraphPad Software;  $p$  = \*, < 0.05; \*\*, < 0.01; \*\*\*, < 0.001).

### SUPPLEMENTAL INFORMATION

Supplemental Information includes six figures and Supplemental Experimental Procedures and can be found with this article online at <http://dx.doi.org/10.1016/j.cmet.2015.03.005>.

### ACKNOWLEDGMENTS

We thank K. Hattori, N. Asinovsky, A. Ortiz-Lopez, K. Leatherbee, D. Jepson, K. Rothamel, S. Davis, H. Paik, R. Cruse, J. LaVecchio, and G. Buruzula for experimental support; C. Shu and D. Burzyn for valuable discussions; and A. Rudensky, V. Kuchroo, O. Kanagawa, R. Lee, and A. MacKenzie for mouse lines. This work was supported by NIH R01DK092541 and the JPB Foundation to D.M., NIH RO1HL088582 to A.J.W., and in part by the Intramural Research Program of NIAID, NIH. Cell sorting was performed at the HSCI/DRC Flow Core (NIH P30DK036836). D.K. and A.M. were supported by fellowships from the National Science and Juvenile Diabetes Research Foundations, respectively. Content is solely the responsibility of the authors and does not represent the official view of the NIH or other funding agencies.

Received: October 2, 2014

Revised: January 12, 2015

Accepted: February 27, 2015

Published: April 7, 2015

### REFERENCES

- Adams, E.J., and Luoma, A.M. (2013). The adaptable major histocompatibility complex (MHC) fold: structure and function of nonclassical and MHC class I-like molecules. *Annu. Rev. Immunol.* **31**, 529–561.
- Bogue, M., Gilfillan, S., Benoist, C., and Mathis, D. (1992). Regulation of N-region diversity in antigen receptors through thymocyte differentiation and thymus ontogeny. *Proc. Natl. Acad. Sci. USA* **89**, 11011–11015.
- Bonilla, W.V., Fröhlich, A., Senn, K., Kallert, S., Fernandez, M., Johnson, S., Kreutzfeldt, M., Hegazy, A.N., Schrick, C., Fallon, P.G., et al. (2012). The alarmin interleukin-33 drives protective antiviral CD8<sup>+</sup> T cell responses. *Science* **335**, 984–989.
- Burzyn, D., Kuswanto, W., Kolodin, D., Shadrach, J.L., Cerletti, M., Jang, Y., Sefik, E., Tan, T.G., Wagers, A.J., Benoist, C., and Mathis, D. (2013). A special population of regulatory T cells potentiates muscle repair. *Cell* **155**, 1282–1295.
- Cipolletta, D., Feuerer, M., Li, A., Kamei, N., Lee, J., Shoelson, S.E., Benoist, C., and Mathis, D. (2012). PPAR- $\gamma$  is a major driver of the accumulation and phenotype of adipose tissue Treg cells. *Nature* **486**, 549–553.
- Cosgrove, D., Gray, D., Dierich, A., Kaufman, J., Lemeur, M., Benoist, C., and Mathis, D. (1991). Mice lacking MHC class II molecules. *Cell* **66**, 1051–1066.
- Darce, J., Rudra, D., Li, L., Nishio, J., Cipolletta, D., Rudensky, A.Y., Mathis, D., and Benoist, C. (2012). An N-terminal mutation of the Foxp3 transcription factor alleviates arthritis but exacerbates diabetes. *Immunity* **36**, 731–741.
- Deng, T., Lyon, C.J., Minze, L.J., Lin, J., Zou, J., Liu, J.Z., Ren, Y., Yin, Z., Hamilton, D.J., Reardon, P.R., et al. (2013). Class II major histocompatibility complex plays an essential role in obesity-induced adipose inflammation. *Cell Metab.* **17**, 411–422.
- Eller, K., Kirsch, A., Wolf, A.M., Sopper, S., Tagwerker, A., Stanzl, U., Wolf, D., Patsch, W., Rosenkranz, A.R., and Eller, P. (2011). Potential role of regulatory T cells in reversing obesity-linked insulin resistance and diabetic nephropathy. *Diabetes* **60**, 2954–2962.
- Feuerer, M., Herrero, L., Cipolletta, D., Naaz, A., Wong, J., Nayer, A., Lee, J., Goldfine, A.B., Benoist, C., Shoelson, S., and Mathis, D. (2009). Lean, but not obese, fat is enriched for a unique population of regulatory T cells that affect metabolic parameters. *Nat. Med.* **15**, 930–939.
- Feuerer, M., Hill, J.A., Kretschmer, K., von Boehmer, H., Mathis, D., and Benoist, C. (2010). Genomic definition of multiple ex vivo regulatory T cell subphenotypes. *Proc. Natl. Acad. Sci. USA* **107**, 5919–5924.
- Garlanda, C., Dinarello, C.A., and Mantovani, A. (2013). The interleukin-1 family: back to the future. *Immunity* **39**, 1003–1018.
- Gerner, M.Y., Kastenmuller, W., Ifrim, I., Kabat, J., and Germain, R.N. (2012). Histo-cytometry: a method for highly multiplex quantitative tissue imaging analysis applied to dendritic cell subset microanatomy in lymph nodes. *Immunity* **37**, 364–376.
- Josefowicz, S.Z., Lu, L.F., and Rudensky, A.Y. (2012a). Regulatory T cells: mechanisms of differentiation and function. *Annu. Rev. Immunol.* **30**, 531–564.
- Josefowicz, S.Z., Niec, R.E., Kim, H.Y., Treuting, P., Chinen, T., Zheng, Y., Umetsu, D.T., and Rudensky, A.Y. (2012b). Extrathymically generated regulatory T cells control mucosal TH2 inflammation. *Nature* **482**, 395–399.
- Malhotra, D., Fletcher, A.L., Astarita, J., Lukacs-Kornek, V., Tayalia, P., Gonzalez, S.F., Elpek, K.G., Chang, S.K., Knoblich, K., Hemler, M.E., et al.; Immunological Genome Project Consortium (2012). Transcriptional profiling of stroma from inflamed and resting lymph nodes defines immunological hallmarks. *Nat. Immunol.* **13**, 499–510.
- Mathis, D. (2013). Immunological goings-on in visceral adipose tissue. *Cell Metab.* **17**, 851–859.
- Miller, A.M., Asquith, D.L., Hueber, A.J., Anderson, L.A., Holmes, W.M., McKenzie, A.N., Xu, D., Sattar, N., McInnes, I.B., and Liew, F.Y. (2010). Interleukin-33 induces protective effects in adipose tissue inflammation during obesity in mice. *Circ. Res.* **107**, 650–658.
- Molofsky, A.B., Nussbaum, J.C., Liang, H.E., Van Dyken, S.J., Cheng, L.E., Mohapatra, A., Chawla, A., and Locksley, R.M. (2013). Innate lymphoid type 2 cells sustain visceral adipose tissue eosinophils and alternatively activated macrophages. *J. Exp. Med.* **210**, 535–549.
- Morris, D.L., Cho, K.W., Delproposto, J.L., Oatmen, K.E., Geletka, L.M., Martinez-Santibanez, G., Singer, K., and Lumeng, C.N. (2013). Adipose tissue macrophages function as antigen-presenting cells and regulate adipose tissue CD4<sup>+</sup> T cells in mice. *Diabetes* **62**, 2762–2772.
- Morton, A.M., Sefik, E., Upadhyay, R., Weissleder, R., Benoist, C., and Mathis, D. (2014). Endoscopic photoconversion reveals unexpectedly broad leukocyte trafficking to and from the gut. *Proc. Natl. Acad. Sci. USA* **111**, 6696–6701.
- Osborn, O., and Olefsky, J.M. (2012). The cellular and signaling networks linking the immune system and metabolism in disease. *Nat. Med.* **18**, 363–374.
- Samstein, R.M., Josefowicz, S.Z., Arvey, A., Treuting, P.M., and Rudensky, A.Y. (2012). Extrathymic generation of regulatory T cells in placental mammals mitigates maternal-fetal conflict. *Cell* **150**, 29–38.
- Schiering, C., Krausgruber, T., Chomka, A., Fröhlich, A., Adelmann, K., Wohlfert, E.A., Pott, J., Griseri, T., Bollrath, J., Hegazy, A.N., et al. (2014). The alarmin IL-33 promotes regulatory T-cell function in the intestine. *Nature* **513**, 564–568.
- Thornton, A.M., Korty, P.E., Tran, D.Q., Wohlfert, E.A., Murray, P.E., Belkaid, Y., and Shevach, E.M. (2010). Expression of Helios, an Ikaros transcription factor family member, differentiates thymic-derived from peripherally induced Foxp3<sup>+</sup> T regulatory cells. *J. Immunol.* **184**, 3433–3441.

- Tomura, M., Yoshida, N., Tanaka, J., Karasawa, S., Miwa, Y., Miyawaki, A., and Kanagawa, O. (2008). Monitoring cellular movement in vivo with photoconvertible fluorescence protein "Kaede" transgenic mice. *Proc. Natl. Acad. Sci. USA* 105, 10871–10876.
- Turnquist, H.R., Zhao, Z., Rosborough, B.R., Liu, Q., Castellana, A., Isse, K., Wang, Z., Lang, M., Stolz, D.B., Zheng, X.X., et al. (2011). IL-33 expands suppressive CD11b<sup>+</sup> Gr-1(int) and regulatory T cells, including ST2L<sup>+</sup> Foxp3<sup>+</sup> cells, and mediates regulatory T cell-dependent promotion of cardiac allograft survival. *J. Immunol.* 187, 4598–4610.
- Wagers, A.J., Sherwood, R.I., Christensen, J.L., and Weissman, I.L. (2002). Little evidence for developmental plasticity of adult hematopoietic stem cells. *Science* 297, 2256–2259.
- Weiss, J.M., Bilate, A.M., Gobert, M., Ding, Y., Curotto de Lafaille, M.A., Parkhurst, C.N., Xiong, H., Dolpady, J., Frey, A.B., Ruocco, M.G., et al. (2012). Neuropilin 1 is expressed on thymus-derived natural regulatory T cells, but not mucosa-generated induced Foxp3<sup>+</sup> T reg cells. *J. Exp. Med.* 209, 1723–1742.
- Wood, I.S., Wang, B., and Trayhurn, P. (2009). IL-33, a recently identified interleukin-1 gene family member, is expressed in human adipocytes. *Biochem. Biophys. Res. Commun.* 384, 105–109.
- Zheng, Y., Josefowicz, S., Chaudhry, A., Peng, X.P., Forbush, K., and Rudensky, A.Y. (2010). Role of conserved non-coding DNA elements in the Foxp3 gene in regulatory T-cell fate. *Nature* 463, 808–812.